The Potent and Selective AMPK Inhibitor BAY-3827 Shows Strong Efficacy in Androgen-Dependent Prostate Cancer Models

Clara Lemos
Bayer AG
Volker K Schulze
Bayer AG
Simon J Baumgart
Bayer AG
Ekaterina Nevedomskaya
Bayer AG
Tobias Heinrich
Bayer AG
Julien Lefranc
ICB Nuvisan
Benjamin Bader
ICB Nuvisan
Clara D Christ
Bayer AG
Hans Briem
Bayer AG
Lara P Kuhnke
Bayer AG
Simon J Holton
ICB Nuvisan
Ulf Bömer
ICB Nuvisan
Philip Lienau
Bayer AG
Franz von Nussbaum
ICB Nuvisan
Carl F Nising
Bayer AG
Marcus Bauser

Bayer AG
Andrea Hägebarth
Bayer AG
Dominik Mumberg
Bayer AG
Bernard Haendler (bernard.haendler@bayer.com)
Bayer Pharma AG https://orcid.org/0000-0002-4490-0663

Research article

Keywords: AMPK, prostate cancer, lipid metabolism

Posted Date: July 29th, 2020

DOI: https://doi.org/10.21203/rs.3.rs-47637/v1

Abstract

Background: 5´ adenosine monophosphate-activated kinase (AMPK) is an essential regulator of cellular energy homeostasis which has been associated with different pathologies, including cancer. Precisely defining the role of AMPK in these processes necessitates the availability of a potent and selective inhibitor.

Methods: High-throughput screening and subsequent chemical optimization led to the identification of the selective inhibitor BAY-3827. Cell proliferation and mechanistic assays, as well as gene expression analysis and chromatin immunoprecipitation were used to investigate the cellular impact of BAY-3827 and the crosstalk between lipid metabolism and androgen signaling in prostate cancer models. Also, fatty acid turnover was determined by examining lipid droplet formation.

Results: BAY-3827 prevented phosphorylation of acetyl-CoA carboxylase 1 and showed strongest anti-proliferative activity in androgen-dependent prostate cancer cell lines. Analysis of genes involved in AMPK signaling revealed that the expression of 3-hydroxy-3-methyl-glutaryl-coenzyme A reductase (HMGCR), fatty acid synthase (FASN) and 6-phosphofructo-2-kinase/fructose-2,6-biphosphatase 2 (PFKFB2), all of which are involved in lipid metabolism, was strongly upregulated by androgen in responsive prostate cancer cell lines. Chromatin immunoprecipitation DNA-sequencing (ChIP-seq) analysis identified androgen receptor (AR) binding peaks in these genes. BAY-3827 strongly down-regulated the expression of lipase E (LIPE), cAMP-dependent protein kinase type II-beta regulatory subunit (PRKAR2B) and serine-threonine kinase AKT3 in the responsive prostate cancer cell lines. Also, the expression of members of the carnitine palmitoyl-transferase 1 (CPT1) family was inhibited by BAY-3827, and this was paralleled by impaired lipid flux.

Conclusions: The availability of the potent and selective inhibitor BAY-3827 will contribute to a better understanding of the biological role of AMPK signaling in cancer, especially in prostate adenocarcinoma.

Background

5´ adenosine monophosphate-activated kinase (AMPK) is a heterotrimeric serine/threonine kinase composed of a catalytic α1 or α2 subunit, a scaffolding β1 or β2 subunit and a regulatory γ1, γ2 or γ3 subunit [1]. It is involved in cellular energy homeostasis and responds to low AMP cellular concentrations by rerouting metabolic processes in order to reduce consumption and increase generation of ATP [1–3]. Additional activation mechanisms such as glucose sensing have also been described, indicating a role beyond coordination of energy homeostasis [4]. The activity of AMPK is critically dependent on the phosphorylation of threonine T172 located in the activation loop of the α subunit, which is controlled by the calcium-calmodulin-dependent kinase 2 (CaMKK2) and the liver kinase B1 (LKB1) [5, 6]. The function of AMPK is tightly regulated by the competitive binding of adenine nucleotides to dedicated AMPK γ subunit sites which regulate access of different protein phosphatases that can reverse T172 phosphorylation. The downstream targets phosphorylated by AMPK are involved in various metabolic

processes. One of the best characterized ones is acetyl-CoA carboxylase 1 (ACC1), a biotin carboxylase and carboxyltransferase involved in fatty acid biosynthesis [7]. A number of other targets, many of which are not involved in cellular metabolism, are phosphorylated by AMPK at a consensus recognition motif [5]. More recently, the role of AMPK in phosphorylating the methylcytosine dioxygenase ten-eleven translocation 2 (TET2) dependent on the extracellular glucose levels, thus leading to epigenetic reprogramming, has been reported [8].

In view of the essential role of AMPK in different cellular processes, it is not surprising that several pathologies including cancer, metabolic dysfunction, inflammatory disorders and neurodegeneration have been associated with this kinase [3, 9–11]. Concerning cancer, pro-tumorigenic and tumor suppressor functions have been reported for AMPK, depending on parameters such as subcellular location, complex members and upstream modulators [12]. A link to MYC oncogenic activity and an impact on anabolic pathways ultimately leading to sustained cell proliferation has been proposed, but details remain to be elucidated [10]. In prostate cancer important metabolic reprogramming takes place and the expression of several main players in this process, including CaMKK2, is controlled by androgens [13]. The role of CaMKK2-AMPK signaling in prostate cancer is gradually being unraveled [14, 15]. This pathway is stimulated during late-stage prostate cancer and may represent an essential survival mechanism [16–19]. Activated AMPK induces autophagy, promotes mitochondrial biogenesis and is involved in apoptosis [18, 20, 21], thereby fostering prostate cancer growth and survival, whereas silencing AMPK expression reduces prostate cancer cell proliferation and migration [13, 22]. However, other studies report that AMPK has a tumor suppressor role in prostate cancer [19, 23–25], so that potent and selective chemical probes [26] will be essential to understand the enigmatic function of AMPK in cancer and other pathologies [2, 3, 9, 12].

AMPK activators mainly bind to the allosteric drug and metabolite site located at the α/β subunit interface and have different isoform selectivity [11]. An inhibitory impact of these compounds on the proliferation of prostate cancer models has been reported but in several cases promiscuous or weak activators were used, which makes interpretation difficult [5, 11, 12]. Data with more selective compounds such as MT 63–78 or 991 also suggest a role of AMPK in impairing prostate cancer cell proliferation, via reduction of lipogenesis and independently of CaMMK2 [24, 25]. A phase 1 clinical study focusing on advanced tumors was initiated with the AMPK activator ASP4132 already several years ago, but only few preclinical data have been reported for this compound [27].

Concerning inhibitors, the pyrazolopyrimidine derivative compound C is a widely used ATP-competitive AMPK inhibitor which however lacks target selectivity, being additionally a strong blocker of different anaplastic lymphoma kinases and also a hinderer of the cellular entry of AICAR, an activator of AMPK [28, 29]. MT 47–100 is both an inhibitor and activator of different AMPK complexes [30]. SU6656 is a Src family kinase also acting as an ATP-competitive AMPK antagonist [31]. SBI-0206965 was originally identified as an Unc-51 like autophagy activating kinase 1 (ULK1) inhibitor [32, 33]. It is a mixed-type inhibitor with IC_{50} values around 330–400 nM for AMPK and 1 μM for ULK1, and blocks downstream cellular signaling [32]. It may however also inhibit additional kinases, as the selectivity panel used to

characterize it only covers 11% of the human kinome [32]. Sunitinib is a multi-kinase inhibitor which also blocks AMPK and derivatives with enhanced AMPK selectivity have very recently been described and tested in a leukemia cell line [34].

Here we describe BAY-3827, a selective and highly potent, low nanomolar inhibitor of AMPK. Profiling in a panel comprising 329 kinases showed only limited off-target activity. Strong cellular activity was demonstrated by determining ACC1 phosphorylation. Proliferation assays revealed that only androgen-dependent prostate cancer cells and mantle lymphoma cells strongly responded to this compound. Analysis focusing on genes involved in AMPK signaling showed the expression of many of them to be highly androgen-dependent. BAY-3827 repressed the expression of several genes involved in lipid metabolism. Consistent with this, the compound strongly impacted lipid turnover in treated prostate cancer cells.

Methods

Compounds and cell lines

BAY-3827 and BAY-974 were synthesized in-house [35] and are available from the Structural Genomics Consortium as donated chemical probes. The androgen R1881 (methyltrienolone) was synthesized in-house. Enzalutamide was purchased from Selleck Chemicals (Houston, TX, USA).

Cell lines were from the American Type Culture Collection (ATCC, Manassas, VA, USA) or the Deutsche Sammlung von Mikroorganismen und Zellkulturen (DSMZ, Braunschweig, Germany), and were routinely grown in the recommended medium at 37 °C and in 5% CO_2 atmosphere. Authentication was performed by the DSMZ using short tandem repeat DNA typing analysis. Cell lines were confirmed to be free of mycoplasma using the MycoAlert Mycoplasma Detection Assay (Lonza, Basel, Switzerland).

Kinase activity assays

A time-resolved fluorescence energy transfer (TR-FRET)-based AMPK activity inhibition assay was established. Full-length human AMPKα2 N-terminally fused to glutathione-S-transferase (GST) was coexpressed with GST-PRKAB1 and PRKAG1 using a baculovirus expression system (#102–114, lot 10CBS-1133D; Carna Biosciences, Kobe, Japan). Purification of the GST-AMPKα2/ß1/γ1 complex was performed using glutathione sepharose chromatography. The biotinylated peptide biotin-Ahx-HMRSAMSFAEPG (C-terminus in amide form) was used as substrate for the kinase reaction (Biosyntan, Berlin, Germany).

For the kinase assay, 50 nl of a 100-fold concentrated solution of the test compound in DMSO were pipetted into either a black low-volume 384-well microtiter plate or a black 1536-well microtiter plate (Greiner Bio-One, Frickenhausen, Germany). Then, 2 µl of a solution of GST-AMPKα2/ß1/γ1 in aqueous assay buffer (50 mM Hepes pH 7.5, 10 mM $MgCl_2$, 5 mM β-glycerophosphate, 2.5 mM dithiothreitol, 0.5 mM EGTA, 0.01% (w/v) bovine γ-globulin, 0.01% (v/v) Triton X-100) were added and the mixture was

incubated for 15 minutes at 22 °C to allow pre-binding of the test compounds to the enzyme. For the kinase reaction with the low adenosine-triphosphate (ATP) condition, ATP was added at a final concentration of 10 µM, adenosine-monophosphate (AMP) at a final concentration of 2 µM and substrate at a final concentration of 0.5 µM in assay buffer, and the resulting mixture was incubated for 90 minutes at 22 °C. For the high ATP condition, ATP was added at a final concentration of 1 mM, AMP at a final concentration of 2 µM and substrate at a final concentration of 0.5 µM in assay buffer, and the resulting mixture was incubated for 30 minutes at 22 °C. The concentration of GST-AMPKα2/ß1/γ1 was adjusted depending on the activity of the preparation batch and was chosen to have the assay in the linear range, a typical concentration being 0.05 nM. The reaction was stopped by addition of 3 µl of a solution of TR-FRET detection reagents (0.2 µM streptavidine-XL665 [Cisbio Bioassays, Codolet, France], 3.33 nM anti-phospho-serine antibody STK [Merck Millipore, Burlington, MA, USA] and 3.33 nM anti-mouse IgG-Tb cryptate, a Terbium-cryptate labelled anti-mouse IgG antibody [Cisbio Bioassays] in an aqueous EDTA solution (166.7 mM EDTA, 0.06% (w/v) bovine serum albumin in 50 mM HEPES pH 7.5). The resulting mixture was incubated for 1 hour at 22 °C to allow the formation of a complex between the phosphorylated biotinylated peptide and the detection reagents. Subsequently the amount of phosphorylated substrate was evaluated by measurement of the resonance energy transfer from the Tb-cryptate to the streptavidine-XL665. For that the fluorescence emissions at 620 nm and 665 nm after excitation at 350 nm were measured in a TR-FRET reader (Pherastar FS, BMG Labtechnologies, Ortenberg, Germany or ViewLux, PerkinElmer, Waltham, MA, USA). The ratio of the emissions was taken as the measure of the amount of phosphorylated substrate. The data were normalized (enzyme reaction without inhibitor = 0% inhibition, all other assay components but no enzyme = 100% inhibition). As a rule, the test compounds were analyzed on the same microtiter plate in 11 different concentrations ranging from 20 µM to 0.07 nM in duplicate values. IC_{50} values were calculated using the Genedata Screener™ software (Basel, Switzerland).

Aurora A kinase activity was determined using N-terminally His-tagged, recombinant protein (Merck Millipore, Burlington, MA, USA) and the biotinylated FMRLRRLSTKYRT peptide (Jerini AG, Berlin, Germany). An anti-phospho-Akt antibody was used for detection, and europium cryptate-labeled protein-A and streptavidin-Xlent! for signal measurement (Cisbio Bioassays). Flt3 kinase activity was determined with N-terminally GST-tagged recombinant protein (Merck Millipore) and the biotinylated GGEEEEYFELVKKKK peptide (Biosyntan). Signal was determined following treatment with PT66-K and streptavidin-Xlent! (Cisbio Bioassays). c-Met kinase activity was determined with in-house produced protein and PolyGT-Biotin (Cisbio Bioassays) as substrate. Signal was measured with Eu-W1024 PT66 (PerkinElmer) and streptavidin-Xlent! (Cisbio Bioassays). Rsk4 activity was determined with 6His-tagged recombinant protein (Eurofins, Brussels, Belgium) and the biotinylated KKLNRTLSFAEPG peptide (Biosyntan). Detection was with an anti-phosphoserine antibody (Amersham Bioscience), and the signal was measured after treatment with Eu-W1024 PT66 (PerkinElmer) and Dy648-conjugated streptavidin (Dyomics GmbH, Jena, Germany). Low ATP concentration (10 µM) was used in these assays.

Selectivity profiling was performed at Eurofins by testing 331 different wild-type human kinases (Additional file 1: Table S1).

Cellular mechanistic assay

The phospho-ACC1 (Ser79) HTRF assay (Cisbio Bioassays) was used to determine the levels of ACC1 phosphorylation in cell lysates. Detection was performed in a sandwich TR-FRET assay using an anti-total ACC1 antibody labeled with the acceptor d2 and an anti-phospho-ACC1 antibody labeled with the donor europium cryptate. On day 1, the cells were seeded in a 384-well Small Volume™ plate (Greiner) in the appropriate culture medium. They were then treated with the inhibitor or DMSO and incubated for 1 hour at 37 °C. Following incubation, the cells were lyzed in 4 µl of lysis buffer for 1 hour on ice. Then 4 µl of antibody solution containing equal amounts of total ACC1 and phospho-ACC1 were added and the samples were incubated overnight at 4 °C. The plate was measured the next day using a PHERAstar FS reader (BMG Labtech, Ortenberg, Germany). IC_{50} values were calculated using the DRC Master Spreadsheet (in-house Bella software) and setting DMSO-treated cells as the minimum inhibition (C0) and staurosporine-treated cells (1 µM of staurosporine) as the maximum inhibition (Ci).

Cell proliferation assays

LNCaP, VCaP, 22Rv1, C4-2B, PC-3 and DU-145 prostate cancer cells were plated at a number of 600, 2,400, 1,200, 600, 600 and 1,000 per well in 384-well white plates in RPMI 1640 medium without phenol red supplemented with 10% charcoal-stripped FBS, except in the case of DU-145 where DMEM/Ham´s F12 medium supplemented with stable glutamine and 10% FBS was used. Sister wells were plated on a separate plate for time zero determination. All plates were incubated overnight at 37 °C. On the next day, the androgen R1881 was added at a final concentration of 1, 0.1, 0.1, 1 and 0.1 nM, except in the case of DU-145 cells. This was followed by addition of the inhibitor in serial dilutions. The plates were incubated at 37 °C for 6 days, except for PC-3 and DU-145 cells where incubation was for 4 and 3 days, respectively. Cell viability was determined with the CellTiter-Glo® assay (Promega, Madison, WI, USA). Luminescence was measured in a Victor X3 reader. Background values measured in wells containing only medium were subtracted from all other values. Control wells containing cells with culture medium, DMSO and R1881 were used to determine the control cell growth at the end of the experiment compared to cells treated only with DMSO.

The following additional cancer cell lines were tested by plating the indicated numbers in 384-well black plates: Oci-Ly-7 (1,000 cells), Ramos (1,000 cells), REC-1 (5,000 cells), RAJI (4,000 cells), SU-DHL-10 (1,000 cells), L-363 (4,000 cells), JJN-3 (1,000 cells), AMO-1 (2,000 cells), SK-N-F1 (1,600 cells), LP-1 (4,000 cells), OPM-2 (4,000 cells), SW780 (2,000), IMR32 (1,600 cells), U251 (2,500 cells), IMR-5/75 (800 cells), MDA-MB-231 (800 cells), MDA-MB-453 (4,000 cells), HeLa (800 cells), Colo201 (800 cells), Colo320 (800 cells), LS-174T (800 cells), SW480 (800 cells), A549 (300 cells), NCI-H292 (500 cells), NCI-H460 (1,000 cells), NCI-H520 (2,000 cells), A2780 (800 cells), BxPC3 (2,500 cells), PANC-1 (900 cells), A375 (4,000 cells), Snu16 (1,000 cells). Alternatively, 96-well plates were used for Daudi (20,000 cells), U2-OS (3,000 cells) and Snu398 (3000 cells) cell proliferation assays. Culture conditions recommended by the

provider were used. Sister wells were plated on a separate plate for time zero determination. All plates were incubated overnight at 37 °C. On the next day, the inhibitor was added in serial dilutions and the plates were incubated at 37 °C for 72 to 144 hours, as detailed (Additional file 2: Table S2). The time zero plate was measured by adding 25 ul/well of CellTiter-Fluor solution (Promega), followed by incubation for 30 minutes at 37 °C and measurement of fluorescence on a PHERAStar reader. After the required incubation time, the plates were measured as described above. Background values measured in wells containing only medium were subtracted from all other values. Control wells containing cells with culture medium and DMSO were used to determine the control cell growth, compared to the initial number of cells (time zero value). To distinguish between cell growth inhibition and cell killing, the fluorescence values were corrected for the mean fluorescence observed for the time zero wells at the day of drug treatment start (time zero value). IC_{50} values were calculated as above.

Immunoblotting

LNCaP cells were grown in 10-cm dishes and treated with 1 nM R1881 for the indicated timepoints. Protein extracts (40 µg) were separated on a NuPAGE 3–8% tris acetate gel (ThermoFisher Scientific, Waltham, MA, USA) and blotted onto a polyvinylidene difluoride membrane (Invitrogen, Carlsbad, CA, USA). Analysis was performed using monoclonal antibodies against ACC1 (#3676), pSer79-ACC1 (#3661), AMPKα (#2532), pThr172-AMPKα (#2535) or HSP90 (#4874) (Cell Signaling Technology, Danvers, MA, USA), or against CaMKK2 (H00010645-M01; Abnova, Taipei City, Taiwan). Detection was performed using the Odyssey Imaging System (LI-COR Biosciences, Lincoln, NE, USA).

Gene expression analysis

LNCaP and VCaP cells were treated with 1 nM R1881, enzalutamide or BAY-3827, as indicated for 24 or 48 hours. RNA was extracted using the RNeasy Plus Mini kit (Qiagen, Hilden, Germany). Synthesis of cDNA was performed with the SuperScript® III First Strand Synthesis SuperMix for qRT-PCR (ThermoFisher). Analysis was performed using the RT^2 Profiler™ PCR Array Human AMPK Signaling 330231 (Qiagen).

Chromatin immunoprecipitation DNA-sequencing (ChIP-seq) and bioinformatics analysis

VCaP cells were treated with 1 nM R1881 and 2 µM enzalutamide, as indicated, for 22 hours. Cells were frozen and sent to Diagenode (Liège, Belgium) for ChIP reactions, as described [36]. Approximately 300 base pair-long DNA fragments were prepared using the Bioruptor Pico with sonication beads (Diagenode). Immunoprecipitation was performed using antibodies specific for the AR (06-680, Merck Millipore). Sequencing reads were mapped to human genome hg19 using the Burrows-Wheeler alignment tool with default settings [37]. Additional steps were performed as recently described [36].

Lipid droplet determination by confocal microscopy and image analysis

Lipid droplet formation was determined using a fluorescent synthetic fatty acid precursor (Red fluorescent BODIPY 558/568 C12, D3835, ThermoFisher) [38]. Briefly, LNCaP cells were cultured in 96-well plates in RPMI1640 supplemented with 10% cFBS and treated with the indicated compounds for 2 or 4 days. Following treatment, they were first incubated for 24 hours with 0.1 µM BODIPY 558/568 C12, then washed with medium and treated for 30 minutes with 4 µM Hoechst 33342 (ThermoFisher) to stain the nuclei, and then fixed with 1% formalin. In the case of VCaP cells, DMEM supplemented with 10% cFBS was used for culture and 1 µM C12 as precursor. This was followed by fixation and washing with 1% cFBS before staining with Hoechst 33342. Imaging was performed with a laser scanning microscope (LSM 700, Carl Zeiss Microscopy, Jena, Germany) using the predefined BTMR (C12 signal) or H342 (Hoechst 33342 signal) channels. Data were analyzed with the ImageJ (National Institute of Health, Bethesda, MD, USA) software and the ratio of lipid droplet to nuclei determined for each experimental condition.

Results

Identification of BAY-3827, a potent and selective small-molecule AMPK inhibitor

A high-throughput biochemical screening was performed to identify AMPK inhibitors. Approximately 4 million compounds were tested and a hit from the dihydropyridine-dicarbonitrile series was selected. Optimization towards potency and selectivity led to the design of BAY-3827 (Fig. 1A). This compound inhibited AMPK kinase activity with IC_{50} values of 1.4 nM at low, 10 µM ATP concentration and 15 nM at high, 2 mM ATP concentration (Table 1). Potential off-target activity was evaluated for Aurora A, Flt3, c-Met and ribosomal S6 kinase (Rsk) 4 which showed IC_{50} values ranging from 36 to 1320 nM (Table 1). Furthermore, a large panel of human, wild-type kinases was then screened in presence of 1 µM BAY-3827 at 10 µM ATP concentration. Inhibition leading to enzymatic activity below 20% of control levels was recorded for only a few kinases (Additional file 1: Table S1). IC_{50} values were then determined to be 9 nM (Rsk1), 52 nM (Rsk2), 24 nM (Rsk3), 43 nM (MSK1) and 94 nM (MST3). Altogether the data showed BAY-3827 to be a potent AMPK inhibitor with over 500-fold selectivity for most of the 331 kinases tested. In order to have a proper negative control we generated BAY-974 (Fig. 1B), which had no inhibitory activity on AMPK, or on Flt3, and only micromolar activity on c-Met (Table 1).

BAY-3827 inhibits cellular AMPK signaling

ACC1 Ser79 phosphorylation was determined to assess the cellular activity of BAY-3827 (Fig. 1C). A strong reduction of phosphorylation was observed in LNCaP and VCaP cells, and to a lesser extent in IMR-32 and especially in Colo320 cells. The negative control BAY-974 had only weak effects on ACC1 Ser79 phosphorylation with IC_{50} values of 4.2 and 6.4 µM in LNCaP and VCaP cells, respectively (not shown).

BAY-3827 shows preferential anti-proliferative activity in androgen-dependent prostate cancer models

The anti-proliferative effects of BAY-3827 were determined in a panel of cancer cell lines. Cell viability was measured after 6 treatment days and strong inhibitory effects were observed for LNCaP and VCaP cells, two prostate cancer cell lines that are responsive to androgen stimulation, whereas no activity was observed in AR-negative prostate cancer cell lines (Fig. 1D). BAY-3827 also showed low micromolar efficacy in multiple myeloma cell lines, but had little impact on a variety of models originating from different hematological and solid tumors (Additional file 2: Table S2). The negative control compound BAY-974 had no anti-proliferative activity on prostate cancer cell lines (Table 2).

Numerous AMPK pathway genes are strongly androgen-regulated

In view of the strong impact of BAY-3827 on prostate cancer models, we further explored the crosstalk between AMPK and androgen signaling in LNCaP cells. Following treatment with different concentrations of the synthetic androgen R1881 for 24, 72 or 144 hours, a dose-dependent phosphorylation increase of ACC1 was observed at the two latest timepoints (Fig. 2A; Additional file 3: Figure S1). This was paralleled by an increase in AMPK phosphorylation and of CaMKK2 protein levels (Fig. 2A; Additional file 3: Figure S1), as reported previously [13, 22].

We further expanded on these findings by determining the impact of androgen treatment on the expression of genes linked to AMPK signaling. RNA was extracted from LNCaP cells treated with DMSO only or with 1 nM R1881 for 24 hours, and analyzed using the AMPK signaling RT^2 array (Additional file 4: Table S3). CAMKK2 was the most strongly upregulated gene with a 3-fold elevated level compared to the DMSO control (Fig. 2B). Expression of the genes for 3-hydroxy-3-methyl-glutaryl-coenzyme A reductase (HMGCR), ACC1, fatty acid synthase (FASN), 6-phosphofructo-2-kinase/fructose-2,6-biphosphatase 2 (PFKFB2) and peroxisome proliferator-activated receptor gamma coactivator 1-beta (PPARGC1B) was regulated over 2-fold (Fig. 2B), and the corresponding proteins are all involved in lipid biosynthesis. Analysis of VCaP cells showed that PFKFB2, HMGCR and FASN expression was also strongly upregulated after 1 nM androgen treatment for 24 or 48 hours, as well as cryptochrome 1 (CRY1), sterol regulatory element-binding transcription factor 1 (SREBF1) and serine/threonine-protein phosphatase 2A catalytic subunit beta isoform (PPP2CB) expression (Fig. 2B). A few other genes were regulated over 2-fold in androgen-treated VCaP cells at single time points (Fig. 2B).

We next looked at AR binding at the most strongly regulated genes. We observed different AR binding peaks which were induced upon androgen application and strongly reduced by additional treatment with the AR antagonist enzalutamide. For CAMKK2, there was a single AR peak immediately upstream of the coding region (Fig. 3A). For HMGCR and PFKFB2, there were several peaks of different intensities all along the respective coding regions (Fig. 3B and 3C). This indicates that the expression of these genes is directly regulated by the AR.

AMPK inhibition down-regulates expression of genes involved in lipid metabolism

We next looked at the direct transcriptional impact of AMPK inhibition on the regulation of selected genes, as before. LNCaP and VCaP cells grown in the presence of R1881 were treated for 24 or 48 hours with BAY-3827. Their RNA was purified and analyzed on the AMPK signaling RT^2 array (Additional file 5: Table S4). A strong, over 10-fold repression of LIPE gene expression was observed in LNCaP cells and 2.5 fold reduction in VCaP cells treated for 24 hours (Fig. 4A and 4B). An 8-fold expression reduction of the serine/threonine kinase AKT3 was furthermore observed in LNCaP cells (Fig. 4A). Expression of cAMP-dependent protein kinase type II-beta regulatory subunit (PRKAR2B), a regulatory subunit of cAMP-dependent protein kinase type II, was halved in LNCaP and in VCaP cells (Fig. 4A and 4B). Expression of several genes from the mitochondrial carnitine palmitoyltransferase (CPT) family which is involved in acyl carnitine formation was also blocked by the AMPK inhibitor in VCaP cells (Fig. 4B and 4C). Importantly, in LNCaP cells, none of the top androgen-stimulated genes was affected by BAY-3827 treatment (Additional file 5: Table S4). In VCaP cells, the situation was somehow different as PRKAR2B and less so carnitine palmitoyl-transferase 1 (CPT1A) expression was inhibited by BAY-3827 treatment (Additional file 5: Table S4). Altogether however, there was no significant correlation between androgen- and AMPK inhibitor-regulated genes, as revealed by scatter plot analysis (Additional file 6: Fig. S2).

AMPK inhibition leads to accumulation of lipid droplets

In view of the strong effects on genes involved in lipid synthesis, we examined the impact of BAY-3827 on fatty acid metabolism. LNCaP and VCaP cells were treated with R1881, and with 1 or 3 μM AMPK inhibitor and 1 μM enzalutamide. BODIPY C12 and Hoechst 33342 were then added and the lipid content in relation to cell nucleus number determined (Fig. 5). The results show that treatment of androgen-stimulated LNCaP or VCaP cells with the AMPK inhibitor BAY-3827 significantly increased the formation of lipid droplets in comparison to androgen treatment only (Fig. 5A and 5B). Co-treatment with BAY-3827 and enzalutamide also led to a significant increase of lipid droplet formation in VCaP cells (Fig. 5B).

Discussion

The role of AMPK as an oncoprotein or a tumor suppressor, depending on the subcellular context, complex formed and upstream regulators, has been reported in several studies [12, 39]. AMPK inhibitors and activators both show anti-proliferative effects, but often these results need to be evaluated with caution, due to the poor efficacy and/or selectivity of many of the compounds evaluated [11, 39]. Here we present the highly potent and selective AMPK inhibitor BAY-3827, which was identified by high-throughput screening followed by compound optimization. It belongs to the dihydropyridine-dicarbonitrile family and had low nanomolar inhibitory activity for AMPK, both in the presence of low and high ATP concentrations. It displayed over 500-fold selectivity over the majority of human kinases tested, the main off-target activity being for FLT3 and for the Rsk family members MSK1 and MST3. The compound

showed cellular activity, as demonstrated by the reduction of pACC1 and pAMPK levels, and of CaMKK2 expression. BAY-3827 exhibited strong anti-proliferative activity only in a subset of tumor models, namely androgen-dependent prostate cancer cell lines and multiple myeloma cell lines.

We focused on prostate cancer models and analyzed the crosstalk between androgen signaling and the AMPK pathway in detail. We found that androgen treatment strongly stimulated the expression of several genes belonging to the AMPK pathway, including many involved in lipid biosynthesis. This was paralleled by an increase of AR peaks in the gene bodies and upstream of the transcription start point, as exemplified for CAMKK2, HMGCR and PFKFB2. CAMKK2 activates AMPK and reduces downstream lipogenesis, but also directly stimulates lipogenesis in an AMPK-independent way [25]. HMGCR plays an essential role in cholesterol biosynthesis and its overexpression has been linked to enzalutamide resistance [40], possibly due to elevated intracrine androgen synthesis [41]. PFKFB2 promotes glucose uptake and subsequent *de novo* lipogenesis in prostate cancer cells [42].

Conversely, AMPK inhibitor treatment blocked many genes involved in lipogenesis. Expression of LIPE, also named hormone-sensitive lipase, was strongly down-regulated by BAY-3827 in both prostate cancer cell lines analyzed. Few functional data are available on the role of this lipase in prostate, but one study shows that it is involved in mitochondrial transport of free cholesterol, upon interaction with the steroidogenic acute regulatory protein [43]. Coculture experiments with adipocytes underline the role of LIPE in lipolytic processes associated with breast cancer cell proliferation [44]. The same study furthermore linked breast cancer growth to increased levels of CPT1A, an enzyme involved in the transport of carnitine into mitochondria. We found CPT1 family members to be down-regulated by BAY-3827, supporting a similar pathway to be implicated in prostate cancer growth. Recent knock-down and overexpression studies underline the role of CPT1 and β-oxidation in prostate cancer growth and treatment resistance [45, 46]. Indeed, the determination of lipid content in treated cells showed that whereas androgen had little direct impact on lipid droplet formation, the treatment with BAY-3827 led to a significant accumulation of intracellular lipids, most likely due to the observed down-regulation of the CPT1 family members. Other genes strongly blocked by BAY-3827 have not been directly linked to lipid metabolism in tumor cells, but essential roles of AKT3 and PRKAR2B in prostate cancer proliferation have been reported [47, 48], suggesting that the inhibitory effects observed for BAY-3827 were potentially also due to the blockade of these genes.

Unlike other tumor types, prostate cancer is not highly dependent on aerobic glycolysis and increased glucose uptake, as evidenced by the poor signals seen in prostate cancer patients when using F-deoxyglucose positron emission tomography [49]. Rather, prostate cancer has a unique dependency on lipid metabolism for energy production, which has been linked to enhanced fatty acid uptake [50], intracrine steroid synthesis and *de novo* fatty acid synthesis [49, 50]. Despite the fact that the expression of many enzymes involved in synthesis, uptake and oxidation of lipids is under androgen control [51, 52] and often upregulated in prostate cancer patients [53, 54], blockade of androgen signaling will eventually cease to be efficacious in prostate cancer patients, suggesting that novel therapeutic agents that address directly lipid metabolism may represent a novel therapeutic opportunity [55]. The present data show that

blockade of lipid metabolism inside prostate tumor cells using the AMPK inhibitor BAY-3827 has the potential to inhibit proliferation and future studies will show how this translates into the clinical setting.

Conclusions

In summary we identified BAY-3827, a potent and selective inhibitor of AMPK. It shows preferential anti-proliferative activity in androgen-dependent prostate cancer models. It regulates the expression of several genes involved in lipid metabolism such as LIPE, PRKAR2B, AKT3 and CPT1 family members. The availability of BAY-3827 will help to better understand the role of AMPK in tumors, especially in prostate adenocarcinoma.

Abbreviations

ACC1: acetyl-CoA carboxylase 1; AMPK: 5´ adenosine monophosphate-activated kinase; AR: androgen receptor; CaMKK2: calcium-calmodulin-dependent kinase 2; ChIP-seq: chromatin immunoprecipitation DNA-sequencing; CPT1: carnitine palmitoyl-transferase 1; CRY1: cryptochrome 1; FASN: fatty acid synthase; GST: glutathione-S-transferase; HMGCR: 3-hydroxy-3-methyl-glutaryl-coenzyme A reductase; HTRF: homogeneous time-resolved fluorescence; LIPE: lipase E; LKB1: liver kinase B1; PFKFB2: 6-phosphofructo-2-kinase/fructose-2,6-biphosphatase 2; PPARGC1B: peroxisome proliferator-activated receptor gamma coactivator 1-beta; PPP2CB: serine/threonine-protein phosphatase 2A catalytic subunit beta isoform; PRKAR2B: cAMP-dependent protein kinase type II-beta regulatory subunit; RSK: ribosomal S6 kinase; SREBF1: sterol regulatory element-binding transcription factor 1; TET2: ten-eleven translocation 2; TR-FRET: time-resolved fluorescence energy transfer; ULK1: autophagy activating kinase 1

Declarations

Ethics approval and consent to participate

Not applicable

Consent for publication

Not applicable

Availability of data and materials

Complete ChIP-seq data are available at NCBI GEO (https://www.ncbi.nlm.nih.gov/geo/) under GSE148358.

Competing interests

All authors are/were employees and/or shareholders of Bayer AG.

Funding

This research received no external funding.

Authors' contributions

Conception and design, CL, VKS, BH; Development of methodology: CL, VKS, BH; Medicinal chemistry and computational chemistry: VKS, TH, JL, HB, LDK, CDC; Acquisition of pharmacology data: CL, SJB, BB, SJH, UB, PL, BH; Analysis and interpretation of data (e.g., statistical analysis, biostatistics, computational analysis): CL, VKS, SJB, EN, BB, CDC, UB, BH; Writing, review, and/or revision of the manuscript: CL, VKS, SJB, EN, BH; Study supervision: CL, VKS, FN, CFN, MB, AH, DM, BH; All authors have read and agreed to the published version of the manuscript.

Acknowledgements

We thank the project team for continuous support. The help of Maria Quanz, Daniel Seifert, Fanny Knoth, Hagen Muckwar, Enrico Spelling, Carolin Pohle, Guido Piechowiak, Sebastian Schulze, Janine Fischer, Vivien Raschke, Pia Stollberg and Daniel Wolleh is gratefully acknowledged. We are indebted to Martin Eilers (University of Würzburg, Germany) for scientific advice.

References

1. Ross FA, MacKintosh C, Hardie DG. AMP-activated protein kinase: a cellular energy sensor that comes in 12 flavours. The FEBS journal. 2016; 283(16):2987-3001.
2. Hardie DG, Schaffer BE, Brunet A. AMPK: An energy-sensing pathway with multiple inputs and outputs. Trends in cell biology. 2016; 26(3):190-201.
3. Carling D. AMPK signalling in health and disease. Current opinion in cell biology. 2017; 45:31-37.
4. Hardie DG. Keeping the home fires burning: AMP-activated protein kinase. Journal of the Royal Society, Interface. 2018; 15(138).
5. Hardie DG, Lin SC. AMP-activated protein kinase - not just an energy sensor. F1000Research. 2017; 6:1724.
6. Kullmann L, Krahn MP. Controlling the master-upstream regulation of the tumor suppressor LKB1. Oncogene. 2018; 37(23):3045-3057.

7. Munday MR, Hemingway CJ. The regulation of acetyl-CoA carboxylase--a potential target for the action of hypolipidemic agents. Advances in enzyme regulation. 1999; 39:205-234.
8. Wu D, Hu D, Chen H, Shi G, Fetahu IS, Wu F, Rabidou K, Fang R, Tan L, Xu S *et al*. Glucose-regulated phosphorylation of TET2 by AMPK reveals a pathway linking diabetes to cancer. Nature. 2018.
9. Umezawa S, Higurashi T, Nakajima A. AMPK: Therapeutic target for diabetes and cancer prevention. Current pharmaceutical design. 2017; 23(25):3629-3644.
10. Haikala HM, Anttila JM, Klefstrom J. MYC and AMPK-Save energy or die! Frontiers in cell and developmental biology. 2017; 5:38.
11. Olivier S, Foretz M, Viollet B. Promise and challenges for direct small molecule AMPK activators. Biochemical pharmacology. 2018; 153:147-158.
12. Khan AS, Frigo DE. A spatiotemporal hypothesis for the regulation, role, and targeting of AMPK in prostate cancer. Nat Rev Urol. 2017; 14(3):164-180.
13. Frigo DE, Howe MK, Wittmann BM, Brunner AM, Cushman I, Wang Q, Brown M, Means AR, McDonnell DP. CaM kinase kinase beta-mediated activation of the growth regulatory kinase AMPK is required for androgen-dependent migration of prostate cancer cells. Cancer research. 2011; 71(2):528-537.
14. Popovics P, Frigo DE, Schally AV, Rick FG. Targeting the 5'-AMP-activated protein kinase and related metabolic pathways for the treatment of prostate cancer. Expert opinion on therapeutic targets. 2015; 19(5):617-632.
15. Awad D, Pulliam TL, Lin C, Wilkenfeld SR, Frigo DE. Delineation of the androgen-regulated signaling pathways in prostate cancer facilitates the development of novel therapeutic approaches. Curr Opin Pharmacol. 2018; 41:1-11.
16. Massie CE, Lynch A, Ramos-Montoya A, Boren J, Stark R, Fazli L, Warren A, Scott H, Madhu B, Sharma N *et al*. The androgen receptor fuels prostate cancer by regulating central metabolism and biosynthesis. The EMBO journal. 2011; 30(13):2719-2733.
17. Karacosta LG, Foster BA, Azabdaftari G, Feliciano DM, Edelman AM. A regulatory feedback loop between Ca2+/calmodulin-dependent protein kinase kinase 2 (CaMKK2) and the androgen receptor in prostate cancer progression. J Biol Chem. 2012; 287(29):24832-24843.
18. Tennakoon JB, Shi Y, Han JJ, Tsouko E, White MA, Burns AR, Zhang A, Xia X, Ilkayeva OR, Xin L *et al*. Androgens regulate prostate cancer cell growth via an AMPK-PGC-1alpha-mediated metabolic switch. Oncogene. 2014; 33(45):5251-5261.
19. Choudhury Y, Yang Z, Ahmad I, Nixon C, Salt IP, Leung HY. AMP-activated protein kinase (AMPK) as a potential therapeutic target independent of PI3K/Akt signaling in prostate cancer. Oncoscience. 2014; 1(6):446-456.
20. Chhipa RR, Wu Y, Ip C. AMPK-mediated autophagy is a survival mechanism in androgen-dependent prostate cancer cells subjected to androgen deprivation and hypoxia. Cellular signalling. 2011; 23(9):1466-1472.
21. Santha S, Viswakarma N, Das S, Rana A, Rana B. Tumor Necrosis Factor-related Apoptosis-inducing Ligand (TRAIL)-Troglitazone-induced apoptosis in prostate cancer cells involve AMP-activated

protein kinase. J Biol Chem. 2015; 290(36):21865-21875.

22. Park HU, Suy S, Danner M, Dailey V, Zhang Y, Li H, Hyduke DR, Collins BT, Gagnon G, Kallakury B *et al*. AMP-activated protein kinase promotes human prostate cancer cell growth and survival. Mol Cancer Ther. 2009; 8(4):733-741.
23. Jurmeister S, Ramos-Montoya A, Neal DE, Fryer LG. Transcriptomic analysis reveals inhibition of androgen receptor activity by AMPK in prostate cancer cells. Oncotarget. 2014; 5(11):3785-3799.
24. Zadra G, Photopoulos C, Tyekucheva S, Heidari P, Weng QP, Fedele G, Liu H, Scaglia N, Priolo C, Sicinska E *et al*. A novel direct activator of AMPK inhibits prostate cancer growth by blocking lipogenesis. EMBO molecular medicine. 2014; 6(4):519-538.
25. Penfold L, Woods A, Muckett P, Nikitin AY, Kent TR, Zhang S, Graham R, Pollard A, Carling D. CAMKK2 promotes prostate cancer independently of AMPK via increased lipogenesis. Cancer research. 2018.
26. Arrowsmith CH, Audia JE, Austin C, Baell J, Bennett J, Blagg J, Bountra C, Brennan PE, Brown PJ, Bunnage ME *et al*. The promise and peril of chemical probes. Nature chemical biology. 2015; 11(8):536-541.
27. Kuramoto K, Yamada H, Shin T, Sawada Y, Azami H, Yamada T, Nagashima T, Ohnuki K. Development of a potent and orally active activator of adenosine monophosphate-activated protein kinase (AMPK), ASP4132, as a clinical candidate for the treatment of human cancer. Bioorg Med Chem. 2020; 28(5):115307.
28. Bain J, Plater L, Elliott M, Shpiro N, Hastie CJ, McLauchlan H, Klevernic I, Arthur JS, Alessi DR, Cohen P. The selectivity of protein kinase inhibitors: a further update. The Biochemical journal. 2007; 408(3):297-315.
29. Fryer LG, Parbu-Patel A, Carling D. Protein kinase inhibitors block the stimulation of the AMP-activated protein kinase by 5-amino-4-imidazolecarboxamide riboside. FEBS letters. 2002; 531(2):189-192.
30. Scott JW, Galic S, Graham KL, Foitzik R, Ling NX, Dite TA, Issa SM, Langendorf CG, Weng QP, Thomas HE *et al*. Inhibition of AMP-activated protein kinase at the allosteric drug-binding site promotes islet insulin release. Chemistry & biology. 2015; 22(6):705-711.
31. Ross FA, Hawley SA, Auciello FR, Gowans GJ, Atrih A, Lamont DJ, Hardie DG. Mechanisms of paradoxical activation of AMPK by the kinase inhibitors SU6656 and sorafenib. Cell chemical biology. 2017; 24(7):813-824 e814.
32. Dite TA, Langendorf CG, Hoque A, Galic S, Rebello RJ, Ovens AJ, Lindqvist LM, Ngoei KRW, Ling NXY, Furic L *et al*. AMP-activated protein kinase selectively inhibited by the type II inhibitor SBI-0206965. J Biol Chem. 2018; 293(23):8874-8885.
33. Egan DF, Chun MG, Vamos M, Zou H, Rong J, Miller CJ, Lou HJ, Raveendra-Panickar D, Yang CC, Sheffler DJ *et al*. Small molecule inhibition of the autophagy kinase ULK1 and identification of ULK1 substrates. Molecular cell. 2015; 59(2):285-297.
34. Matheson CJ, Casalvieri KA, Backos DS, Minhajuddin M, Jordan CT, Reigan P. Substituted oxindol-3-ylidenes as AMP-activated protein kinase (AMPK) inhibitors. Eur J Med Chem. 2020; 197:112316.

35. Schulze VK, Heinrich T, Christ C, Briem H, Faria Alvares de Lemos AC, Bader B, Holton S, Bömer U, Lienau P, Kuhnke LP. 2019; Patent application WO2019/185525:A1.
36. Baumgart SJ, Nevedomskaya E, Lesche R, Newman R, Mumberg D, Haendler B. Darolutamide antagonizes androgen signaling by blocking enhancer and super-enhancer activation. Mol Oncol. 2020.
37. Li H, Durbin R. Fast and accurate short read alignment with Burrows-Wheeler transform. Bioinformatics. 2009; 25(14):1754-1760.
38. Wang H, Wei E, Quiroga AD, Sun X, Touret N, Lehner R. Altered lipid droplet dynamics in hepatocytes lacking triacylglycerol hydrolase expression. Mol Biol Cell. 2010; 21(12):1991-2000.
39. Vara-Ciruelos D, Russell FM, Hardie DG. The strange case of AMPK and cancer: Dr Jekyll or Mr Hyde? Open Biol. 2019; 9(7):190099.
40. Kong Y, Cheng L, Mao F, Zhang Z, Zhang Y, Farah E, Bosler J, Bai Y, Ahmad N, Kuang S *et al*. Inhibition of cholesterol biosynthesis overcomes enzalutamide resistance in castration-resistant prostate cancer (CRPC). J Biol Chem. 2018; 293(37):14328-14341.
41. Liu C, Lou W, Zhu Y, Yang JC, Nadiminty N, Gaikwad NW, Evans CP, Gao AC. Intracrine androgens and AKR1C3 activation confer resistance to enzalutamide in prostate cancer. Cancer research. 2015; 75(7):1413-1422.
42. Moon JS, Jin WJ, Kwak JH, Kim HJ, Yun MJ, Kim JW, Park SW, Kim KS. Androgen stimulates glycolysis for de novo lipid synthesis by increasing the activities of hexokinase 2 and 6-phosphofructo-2-kinase/fructose-2,6-bisphosphatase 2 in prostate cancer cells. The Biochemical journal. 2011; 433(1):225-233.
43. Locke JA, Guns ES, Lehman ML, Ettinger S, Zoubeidi A, Lubik A, Margiotti K, Fazli L, Adomat H, Wasan KM *et al*. Arachidonic acid activation of intratumoral steroid synthesis during prostate cancer progression to castration resistance. Prostate. 2010; 70(3):239-251.
44. Balaban S, Shearer RF, Lee LS, van Geldermalsen M, Schreuder M, Shtein HC, Cairns R, Thomas KC, Fazakerley DJ, Grewal T *et al*. Adipocyte lipolysis links obesity to breast cancer growth: adipocyte-derived fatty acids drive breast cancer cell proliferation and migration. Cancer Metab. 2017; 5:1.
45. Flaig TW, Salzmann-Sullivan M, Su LJ, Zhang Z, Joshi M, Gijon MA, Kim J, Arcaroli JJ, Van Bokhoven A, Lucia MS *et al*. Lipid catabolism inhibition sensitizes prostate cancer cells to antiandrogen blockade. Oncotarget. 2017; 8(34):56051-56065.
46. Joshi M, Stoykova GE, Salzmann-Sullivan M, Dzieciatkowska M, Liebman LN, Deep G, Schlaepfer IR. CPT1A supports castration-resistant prostate cancer in androgen-deprived conditions. Cells. 2019; 8(10).
47. Lin HP, Lin CY, Huo C, Jan YJ, Tseng JC, Jiang SS, Kuo YY, Chen SC, Wang CT, Chan TM *et al*. AKT3 promotes prostate cancer proliferation cells through regulation of Akt, B-Raf, and TSC1/TSC2. Oncotarget. 2015; 6(29):27097-27112.
48. Sha J, Xue W, Dong B, Pan J, Wu X, Li D, Liu D, Huang Y. PRKAR2B plays an oncogenic role in the castration-resistant prostate cancer. Oncotarget. 2017; 8(4):6114-6129.

49. Eidelman E, Twum-Ampofo J, Ansari J, Siddiqui MM. The metabolic phenotype of prostate cancer. Front Oncol. 2017; 7:131.
50. Liu Y, Zuckier LS, Ghesani NV. Dominant uptake of fatty acid over glucose by prostate cells: a potential new diagnostic and therapeutic approach. Anticancer Res. 2010; 30(2):369-374.
51. Galbraith L, Leung HY, Ahmad I. Lipid pathway deregulation in advanced prostate cancer. Pharmacol Res. 2018; 131:177-184.
52. Tousignant KD, Rockstroh A, Taherian Fard A, Lehman ML, Wang C, McPherson SJ, Philp LK, Bartonicek N, Dinger ME, Nelson CC *et al*. Lipid uptake Is an androgen-enhanced lipid supply pathway associated with prostate cancer disease progression and bone metastasis. Mol Cancer Res. 2019; 17(5):1166-1179.
53. Wu X, Daniels G, Lee P, Monaco ME. Lipid metabolism in prostate cancer. Am J Clin Exp Urol. 2014; 2(2):111-120.
54. Giunchi F, Fiorentino M, Loda M. The metabolic landscape of prostate cancer. Eur Urol Oncol. 2019; 2(1):28-36.
55. Stoykova GE, Schlaepfer IR. Lipid metabolism and endocrine resistance in prostate cancer, and new opportunities for therapy. Int J Mol Sci. 2019; 20(11).

Tables

Table 1
Kinase inhibitory activity of BAY-3827 and BAY-974

	IC_{50} (nM)					
	AMPK (low)	**AMPK (high)**	**Aurora A**	**Flt3**	**c-Met**	**Rsk4**
BAY-3827	1.4 ±0.6	15 ±10	1324 ±272	124 ±140	788 ±120	36 ±8
BAY-974	> 20000	> 20000	n.d.	> 20000	8350±71	n.d
Mean IC_{50} ±SD values are given from at least 6 biological replicates for BAY-3827, and for 2 biological replicates for BAY-974 . n.d.: not determined.						

Table 2
Anti-proliferative activity of BAY-3827 and BAY-974 in prostate cancer cell lines

	IC_{50} (nM)					
	LNCaP	**VCaP**	**22Rv1**	**C4-2B**	**PC-3**	**DU-145**
BAY-3827	0.28±0.11	1.71±0.28	5.55±1.77	> 10	> 10	> 10
BAY-974	> 10	> 10	> 10	> 10	> 10	> 10
Mean IC_{50} ±SD values from at least 2 biological replicates are given.						

Figures

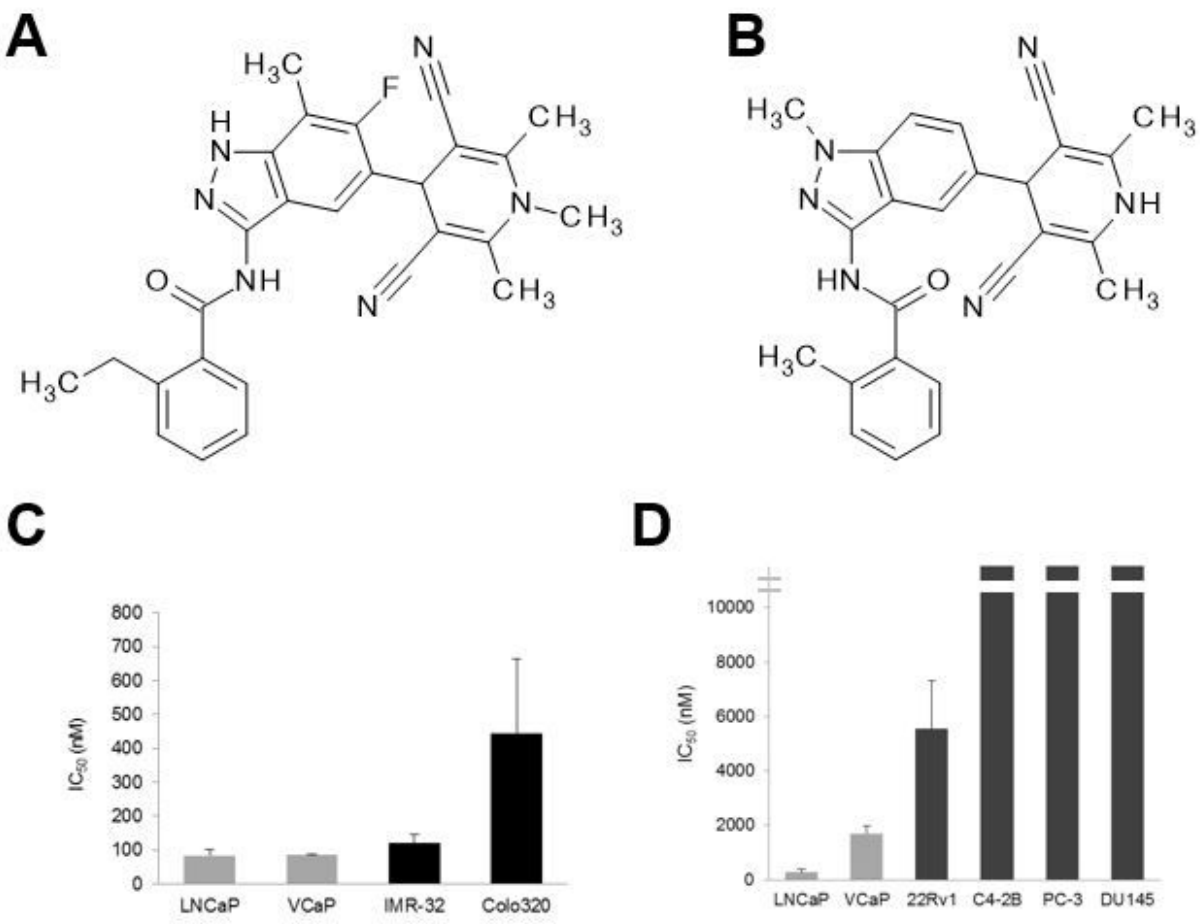

Fig. 1

Figure 1

Androgen-dependent prostate cancer cell lines are sensitive to AMPK inhibition. A Chemical structure of the AMPK inhibitor BAY-3827. B Chemical structure of BAY-974, a structurally related inactive compound. C Cellular AMPK signaling measured by assessing ACC1 Ser79 phosphorylation with a TR-FRET assay following treatment with a dose-range of BAY-3827 overnight. Data represent mean IC50 ± SD. D Prostate cancer cell viability determined by CellTiter-Glo® after treatment with a dose-range of BAY-3827 for 6 days. Data represent mean IC50 ± SD.

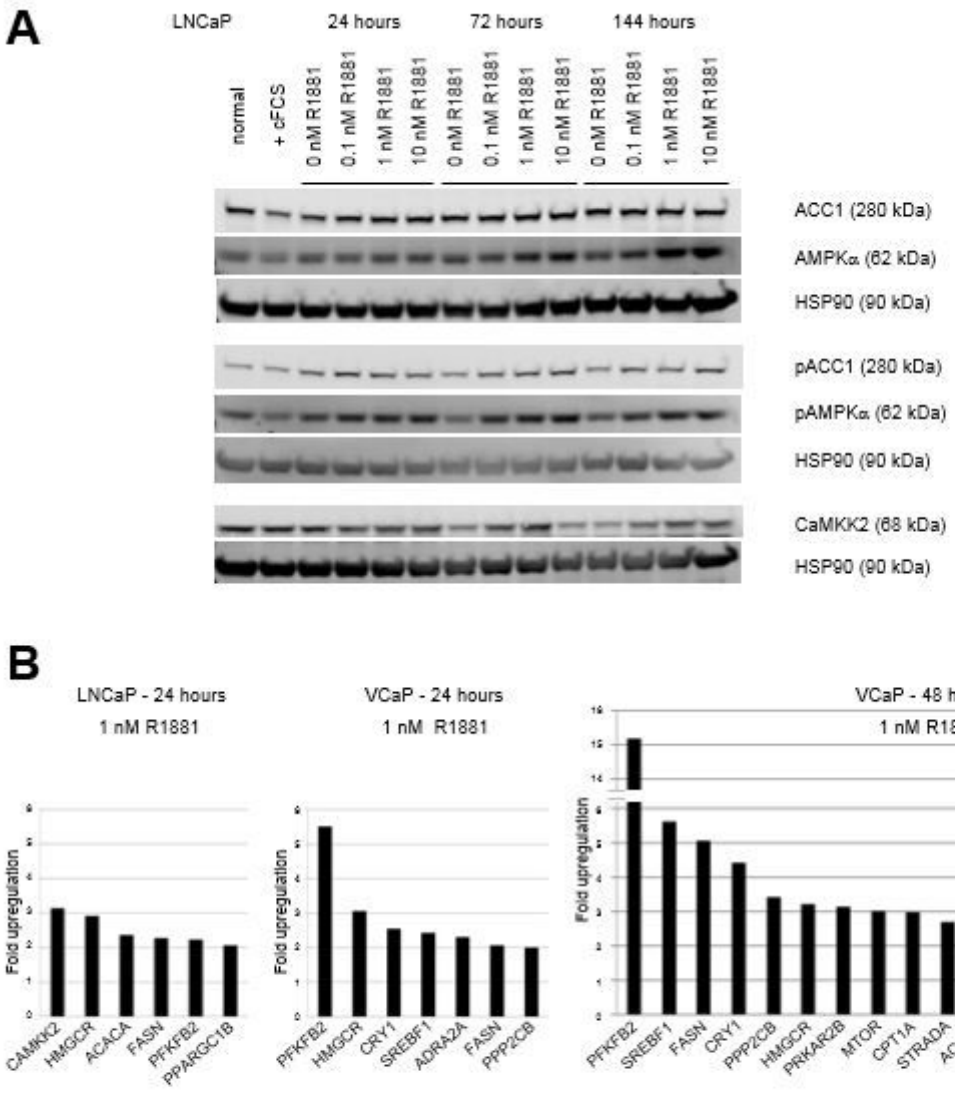

Fig. 2

Figure 2

Impact of androgen treatment on AMPK signaling in prostate cancer cell lines. A Western blot analysis of ACC1, AMPKa, CaMKK2 protein levels, and of ACC1 and AMPKa phosphorylation. B Expression analysis of genes involved in AMPK signaling using the RT2 ProfilerTM PCR array.

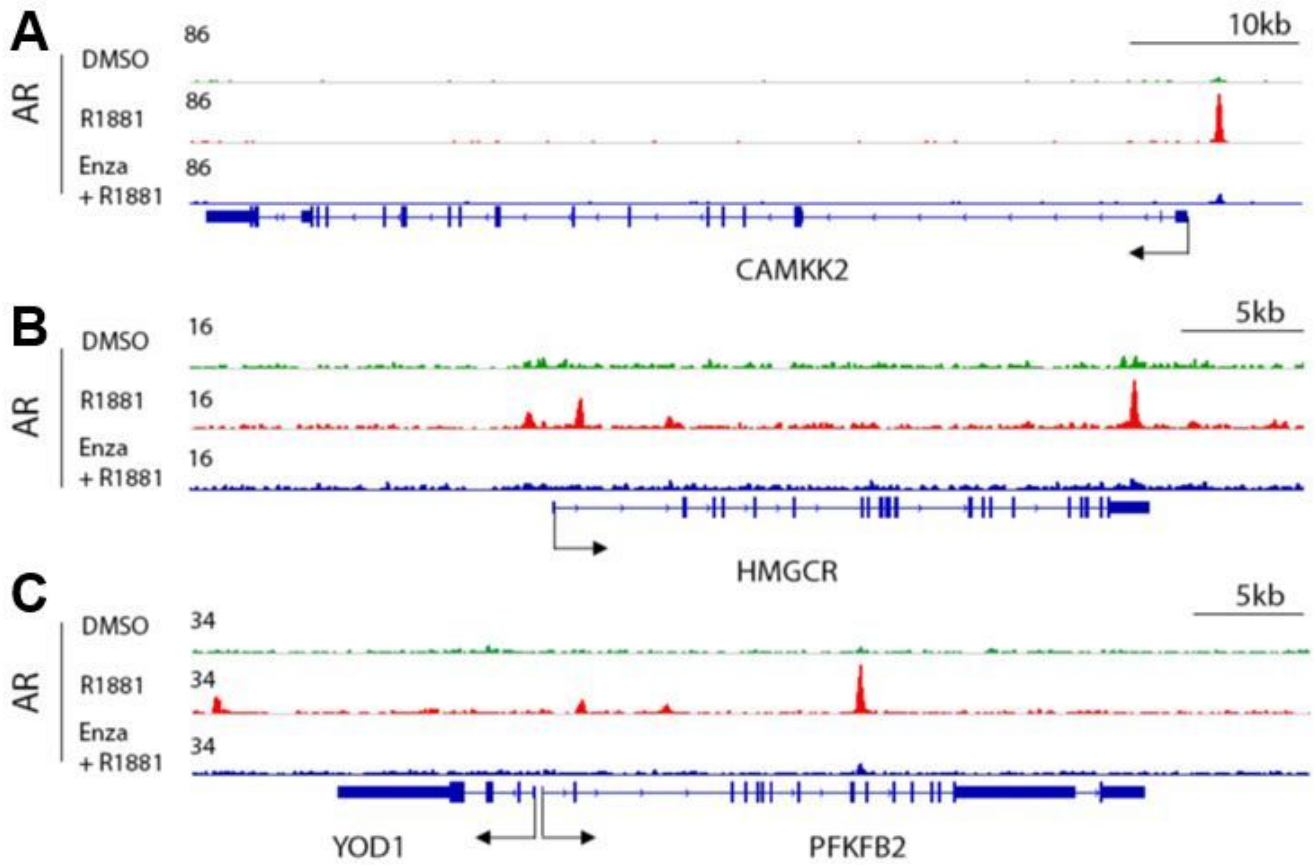

Fig. 3

Figure 3

Androgen-dependent AR binding at regulated genes. A CAMKK2 gene coding region. B HMGCR gene coding region. C PFKFB2 gene coding regions. AR ChIP-seq signals are shown for VCaP cells treated for 22 hours with DMSO, 1 nM R1881 or 1 nM R1881 plus 2 μM enzalutamide (Enza).

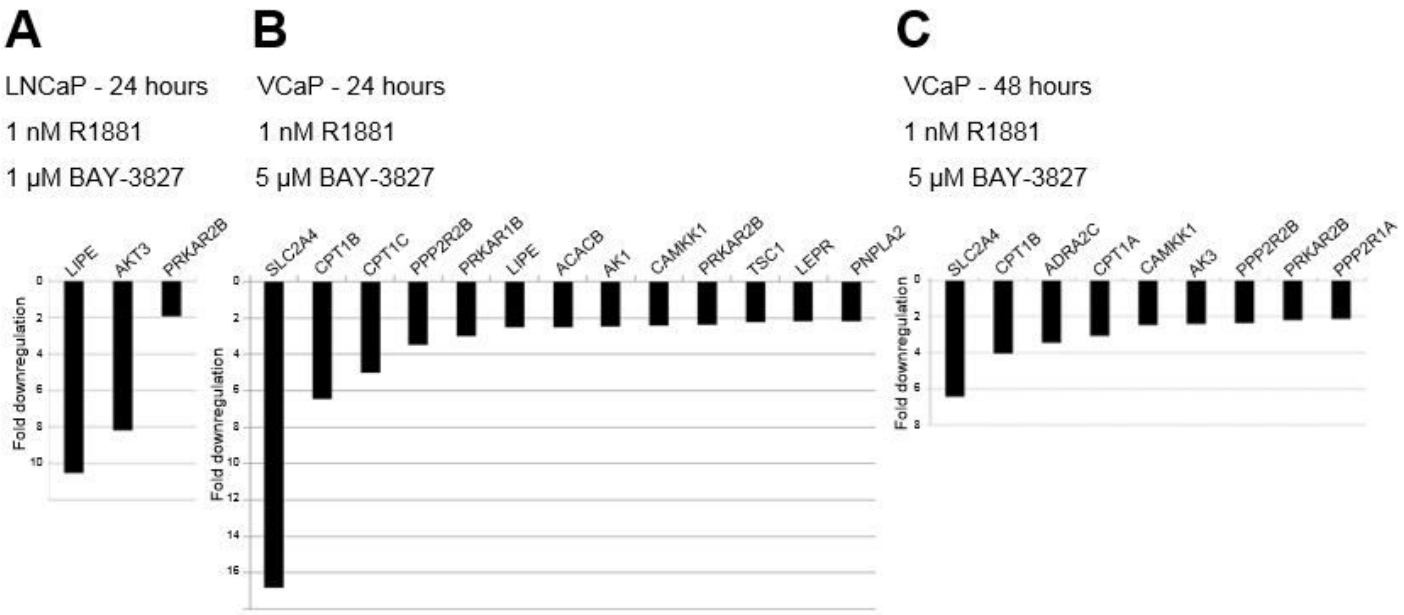

Fig. 4

Figure 4

Impact of BAY-3827 on AMPK signaling in prostate cancer cell lines. A LNCaP cell line. B and C VCaP cell line. Treatment conditions are indicated. Expression of genes involved in AMPK signaling were analyzed using the RT2 ProfilerTM PCR array.

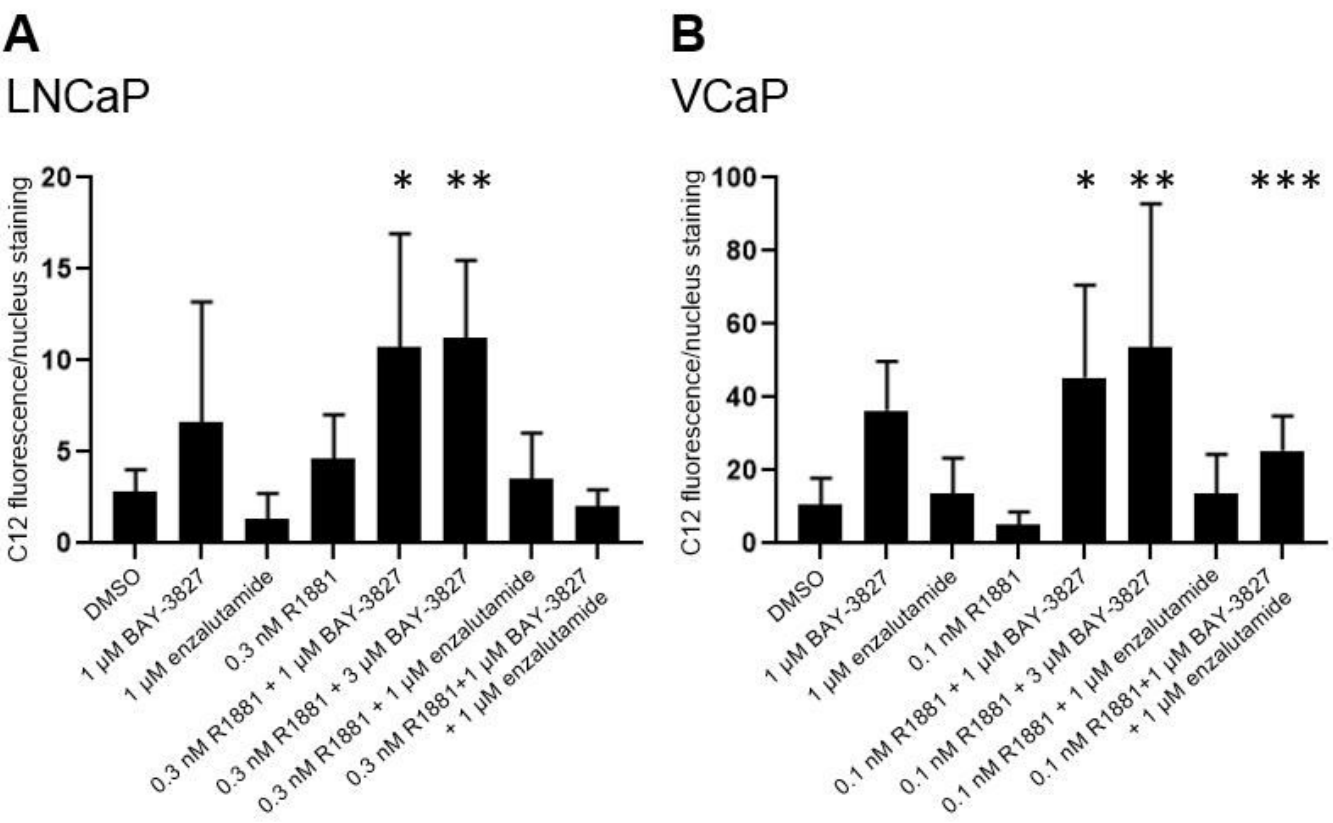

Fig. 5

Figure 5

Impact of BAY-3827 on lipid droplet formation. Cells were incubated with the fatty acid precursor BODIPY 558/568 C12 and treated as indicated. Fluorescence was determined by laser scanning microscopy and shown in relation to the signals measured after nucleus staining. A Ratio of lipid droplets to nuclei in LNCaP cells treated as indicated. *p=0.0445, **p=0.0069 compared to R1881-treated group using Dunnett´s multiple comparison test. B Ratio of lipid droplets to nuclei in VCaP cells treated as indicated. *p=0.0044, **p=0.0230, ***p=0.0012 compared to R1881-treated group using Dunnett´s multiple comparison test.

Supplementary Files

This is a list of supplementary files associated with this preprint. Click to download.

- AMPKiSupplFilesBMCCancer.pptx